Applied Catalysis B: Environmental 232 (2018) 454–463

Contents lists available at ScienceDirect

Applied Catalysis B: Environmental

journal homepage: www.elsevier.com/locate/apcatb

In situ ATR-IR studies in aqueous phase reforming of hydroxyacetone on Pt/ZrO_2 and Pt/AlO(OH) catalysts: The role of aldol condensation

Kamila Koichumanova[a], Anna Kaisa K. Vikla[a], Remedios Cortese[b], Francesco Ferrante[b], K. Seshan[a], Dario Duca[b], Leon Lefferts[a,*]

[a] Catalytic Processes and Materials group, Mesa+ Institute for Nanotechnology, University of Twente, PO Box 217, 7500 AE Enschede, The Netherlands
[b] Dipartimento di Fisica e Chimica, Università degli Studi di Palermo, Viale delle Scienze, ed. 17, 90128, Palermo, Italy

ARTICLE INFO

Keywords:
ATR-IR spectroscopy
In situ
Aqueous phase reforming
Aldol condensation
Liquid phase

ABSTRACT

In situ Attenuated Total Reflection Infrared (ATR-IR) spectroscopy was used to study Aqueous Phase Reforming of hydroxyacetone on Pt/AlO(OH) and Pt/ZrO_2 catalysts at 230 °C/ 30 bar. Formation of strongly adsorbed aldol condensation products was observed on the surface of Pt/ZrO_2 and ZrO_2 in contrast to Pt/AlO(OH) and AlO(OH). Peak assignments were supported by DFT calculations of the IR spectra of the condensation products in vacuum and in the presence of water. Aldol condensation of hydroxyacetone leading to compounds with high molecular weight with unsaturated bonds was suggested as a first step in coke formation. Carbonaceous deposits on the surface of the ZrO_2 support are oxygen-rich and highly reactive, according elemental analysis and TPO. Surprisingly, no adsorbed CO on Pt was observed in the spectra obtained under reaction conditions, suggesting that adsorbed CO is not involved in the rate-determining step in APR of hydroxyacetone.

1. Introduction

Depletion of fossil energy resources have given rise to large number of investigations on development of processes based on alternative energy resources such as biomass, solar and wind energy. Biomass flash-pyrolysis is one of the promising processes for production of bio-oil, an alternative to crude oil, which can be further used for the production of fuels and chemicals. The aqueous phase, containing up to 20% of different organic compounds, is a by-product of biomass pyrolysis, which is currently considered a waste.

Aqueous phase reforming (APR) process [1,2] was suggested for utilization of such streams allowing the production of hydrogen or alkanes at milder temperatures as compared to steam reforming (SR). There is no need for evaporation of water, which saves on energy usage, and the process conditions (150–300 °C, up to 100 bar) are favoring Water Gas Shift (WGS) reaction, maximizing the hydrogen yield. Pt/γ-Al_2O_3 catalyst has been used as a benchmark catalyst in APR of various oxygenates containing more than one carbon atom, e.g., glycerol, sorbitol, acetic acid, acetone, due to ability of Pt to cleave C—C bonds. This cleavage leads to the formation of C_1 species, which are the intermediate species for CO_x or methane [3,4]. However, hot compressed water conditions used in APR lead to transformation of alumina support into a hydrated phase, known as boehmite, resulting in catalyst deactivation [5–7]. Thus, hydrothermally stable supports such as carbon [8–10], zirconia or boehmite are preferred as catalyst supports. It has been shown that Pt/AlO(OH) catalyst is active in APR of ethylene glycol with an appreciably high selectivity to hydrogen [6].

The majority of APR studies use alcohols (e.g., methanol, ethanol) or polyols (glycerol, sorbitol) as model compounds as reviewed recently by Coronado et al. [11] However, the aqueous phase of bio-oil also contains large amounts of organic acids, aldehydes and ketones, which are less studied. Hydroxyacetone (1-hydroxy-2-propanone or acetol) is a component present in significant concentration (3–8 wt. %) [12,13] in aqueous phase of bio-oil. The APR of hydroxyacetone has not yet been studied, particularly using ZrO_2 and/or AlO(OH) supported Pt catalysts. However, few studies are available on SR of bio-oil derived light oxygenates such as hydroxyacetone, acetic acid, furfural, 1-propanol, *n*-butanol, propanal and acetone [14–19] using base metal catalysts. SR of hydroxyacetone at lower temperatures (< 600 °C) resulted in the formation of oxygenated by-products, such as, butanediol, 2,5-hexanediol, substituted cyclopentanedione and furanones, suggesting that condensation reactions leading to larger compounds take place parallel to C—C bond breaking leading to C_1 compounds, i.e. CO_x and CH_4 [14]. Ongoing research in our group on kinetics of APR of hydroxyacetone using Pt/ZrO_2 and Pt/AlO(OH) showed deactivation of both catalysts during the reaction, caused by i.e. coke deposition.

In general, spectroscopic investigation, particularly with IR spectroscopy [20] has provided important information on adsorption of

* Corresponding author.
E-mail address: l.lefferts@utwente.nl (L. Lefferts).

https://doi.org/10.1016/j.apcatb.2018.03.090
Received 2 January 2018; Received in revised form 14 March 2018; Accepted 25 March 2018
Available online 27 March 2018

reactants and intermediates at the surface of catalysts. More recently, this approach has become also available for catalytic reaction in liquid phase [21–23] by using in situ ATR-IR spectroscopy. ATR-IR spectroscopy is suppressing the contribution of the solvent to the IR spectra compared to other types of IR cells, allowing identification of surface species adsorbed on the catalyst. Even more recently, this technique has been adapted to allow experiments in hot compressed water, enabling application during APR of hydroxyacetone at 230 °C and 30 bar [7,24].

In this study, the adsorption of hydroxyacetone on Pt/ZrO_2 and Pt/AlO(OH) catalysts under APR conditions, i.e. 230 °C/30 bar, is studied using in situ ATR-IR spectroscopy. The goal of the investigation is to detect and identify surface species formed as a result of hydroxyacetone adsorption and further transformations into desired or undesired products. Correlation between the structure of the surface species observed by ATR-IR and a possible route of catalyst deactivation will be made.

2. Experimental

2.1. Catalyst preparation

Catalysts were prepared by wet impregnation of commercial monoclinic ZrO_2 (RC100, Gimex Technisch Keramik B.V.) and boehmite (AlO(OH)) supports, the latter made by subjecting γ-alumina (BASF) to hydrothermal conditions, i.e., 200 °C, 14 bar for 10 h in an autoclave. $H_2PtCl_6{\cdot}6H_2O$ (Alfa Aesar) was used as a platinum precursor. Supports (300–600 μm fraction) were added to an aqueous solution of the precursor (H_2O to catalyst weight ratio of 1,8) followed by evaporation of water in a rotary evaporator under vacuum at 100 °C. Samples were then reduced in H_2 atmosphere (H_2 100 mL/min, N_2 100 mL/min) at 100 °C for 5 h and calcined in air (200 mL/min) at 350 °C (5 °C/min) for 15 h.

2.2. Catalyst characterization

The surface areas of the catalysts were measured by N_2 physisorption using the BET adsorption isotherm (Micromeritics, ASAP 2400). The Pt dispersion was established by H_2 pulse chemisorption at room temperature (Micromeritics, Chemisorb 2750), after samples were reduced in pure H_2 at 200 °C for 1 h. TEM microscopy (Philips 300 kV, equipped with energy-dispersive X-Ray spectroscopy) was used to determine the Pt particle size distribution of fresh and spent catalysts. Approximately 250 particles across 10 different spots on each sample were measured to give a weighted average size.

The elemental composition of the catalysts was determined using a Perkin-Elmer elemental analyser (Thermo Scientific Flash 2000). Approximately 3–4 mg of each sample was used for the analysis. Concentrations of C, H and N were calculated based on amounts of water, CO_2 and N_2 evolved from decomposition of the sample in 35 vol. % O_2/Ar flow (390 mL/min) at 900 °C. Acetanilide was used for calibration, and oxygen content was calculated as rest.

Temperature Programmed Oxidation was used to determine the type of coke deposits on the spent catalysts. Samples (3–4 mg) were pretreated in He (25 mL/min) at 150 °C for 30 min. After cooling down to 25 °C the samples were oxidized in 5 vol. % O_2/He mixture (25 mL/min) during heating to 600 °C with a heating rate of 5 °C/min. An online methanizer (Model 110 Chassis, SRI Instruments Europe GmbH) was used to convert CO and CO_2 to methane using a Ni catalyst. The amount of methane formed was quantified with an FID detector. $Al_2(CO_3)_3$ was used for calibration of the FID.

2.3. Acidity measured by NH_3 TPD and Pyridine adsorption IR spectroscopy

Fourier transform infrared spectroscopy (FTIR) of adsorbed pyridine was conducted in a Bruker IFS 66 spectrometer equipped with HgCdTe detector (4000–650 cm^{-1}, 2 cm^{-1} resolution, 32 scans). Prior to pyridine adsorption at room temperature, self-supporting wafers of Pt/ZrO_2 and Pt/AlO(OH) (5 ton/cm^2, 20 mg, 1 cm^2) were degassed under vacuum (10^{-3} mbar) for 2 h at 200 °C. Gaseous and weakly adsorbed pyridine was removed by evacuation for 30 min at 25 °C. To evaluate the adsorption strength of chemisorbed pyridine, catalysts were subsequently treated at 225 °C for 60 min.

Temperature-programmed desorption of ammonia (NH_3-TPD) was performed in a Autochem 2910 II instrument from Micromeritics. The samples were pretreated in He (50 mL/min) at 200 °C for 1 h. NH_3 adsorption was performed at room temperature for 30 min, followed by removal of physisorbed NH_3 in He flow for 1 h. Desorption of NH_3 was monitored in the range of 20–600 °C using a heating rate of 10 °C/min.

2.4. In situ ATR-IR spectroscopy

In situ ATR-IR experiments were performed using a setup consisting of a commercial ATR-IR Tunnel cell (Axiom) modified for high temperature and pressure conditions [24], which was mounted in a sample chamber of an FTIR spectroscopy bench (Bruker, Tensor 27) equipped with liquid-nitrogen cooled HgCdTe detector.

The cylindrical internal reflection element (IRE, ZnSe rod, diameter 0.25 inch, length 3.25 inch) was spray-coated with a catalyst slurry (0.150 g in 25 mL of isopropanol, ball-milled for 6 min) according to a home-developed spray-coating technique [6,24]. The sample was then carefully placed inside the cell using O-rings (Kalrez 7075) and dried at 150 °C in He (25 mL/min) for 1.5 h.

Spectra were recorded every minute in the spectral range between 4000 and 650 cm^{-1} with a resolution of 4 cm^{-1} averaging over 139 scans. The spectrum in He (25 mL/min) (average of 256 scans) of catalyst/support layer was used as background. Penetration depths of IR light were calculated for Pt/AlO(OH), Pt/ZrO_2, AlO(OH) and ZrO_2 according to Mojet et al. [21]

Results showed no difference between the samples with and without Pt. Penetration depths for Pt/AlO(OH) and Pt/ZrO_2 were 0.89 and 0.77 μm, respectively, showing only 15% difference between two samples. Thus, small variations in the IR intensity in spectra of the two samples should be expected.

For all ATR-IR experiments, the cell was first filled with water (2 mL/min) using HPLC pump (Dionex P680), and the sample was subjected to a cleaning procedure adopted from literature [25]. In our experiments this procedure consisted of alternating flows of hydrogen-, oxygen- and helium-saturated water (2 mL/min, 30 min each flow) at ambient conditions. Hydrogen-saturated water was used in the final treatment in order to leave the sample in reduced state. Finally, water was flown over the sample again and pressure was increased to the desired experimental pressure (20 or 30 bar) using back-pressure regulator. After that, the cell and the preheater lines were heated to the desired experiment temperature (100 °C or 230 °C) and a spectrum of water was collected. The flow was then switched to the degassed hydroxyacetone solution (2.5 wt.%, 0.8 mL/min) with simultaneous acquisition of ATR-IR spectra for 60 min. Further, the flow was switched back to water (0.8 mL/min) and ATR-IR spectra were collected for another hour.

For CO adsorption experiments, water saturated with CO (1 bar) at room temperature was flown over the sample at room temperature for 60 min, then the sample was heated to 230 °C, 30 bar during continuous feeding of CO-containing water. After reaching 230 °C, spectra were collected for 60 min. A pretreatment procedure as described above was applied.

2.5. ATR-IR data processing

In situ ATR-IR spectra were first pre-processed (subtraction of water and catalyst spectrum, baseline correction) using OPUS software provided together with the Bruker FTIR spectrometer. Water and catalyst subtraction was performed for all spectra using the respective spectrum of water at the temperature of the experiment. Baseline correction was

done for all spectra using rubber-band correction method. Deconvolution of the spectra was performed using Matlab software. The spectra were fitted using Gaussian peak shapes with fixed peak positions assigned to specific relevant species. However, minor peaks present in the spectral range, but not relevant to hydroxyacetone reaction, have to be included to obtain good quality fit.

2.6. DFT calculations of IR spectra

To support assignments of the IR peaks observed during the experiments, IR spectra of hydroxyacetone, its enols and products of aldol condensation of hydroxyacetone were calculated in vacuum and in the presence of water. All calculations have been performed using Density Functional Theory with the Becke three-parameters (B3LYP) exchange-correlation functional using the Gaussian 09 program [26]. The geometry of all the investigated components has been optimized by employing the correlation consistent polarized valence triple zeta (cc-pVTZ) basis set and the same has been used to calculate harmonic vibrational frequencies.

In order to achieve a more reliable comparison with the experimental spectra, anharmonicity has been taken into account by the following procedure. Since the direct calculation of the anharmonic frequencies of medium sized molecules at the B3LYP/cc-pVTZ level is a demanding task, they have been evaluated with the less extended cc-pVDZ basis set, using optimized geometries at the same level. Anharmonicity corrections have been obtained as the differences between the harmonic and fundamental frequencies, and these corrections were then applied to the harmonic cc-pVTZ frequencies. The reliability of these composite TZ + DZ anharmonic frequency calculations has been checked by comparing them with the entirely TZ anharmonics calculated for the smaller species investigated in this work (hydroxyacetone in all its conformations and tautomers) in the frequency range 4000–400 cm^{-1}. The results showed that the composite TZ + DZ anharmonics represent a good improvement over the purely DZ ones and they have a mean absolute percent deviation of only 0.9% with respect to the full TZ fundamentals. Furthermore, a comparison with the experimental data for hydroxyacetone in its most stable conformation yields the following results for the root mean square deviations: RMSD(TZ) = 20, RMSD(DZ) = 34, RMSD(TZ + DZ) = 24 cm^{-1}, which clearly demonstrates excellent reliability of the composite approach for the hydroxyacetone spectrum. Therefore, it was assumed that the TZ + DZ protocol worked well also for the larger molecular systems in this study.

3. Results

3.1. Catalyst characterization

Two catalysts were used in the study - Pt/AlO(OH) with BET surface area of 41 m^2/g and Pt particles of 5 nm and Pt/ZrO_2 with BET surface area of 94 m^2/g and Pt particles of 1.8 nm. Pt loading for both catalysts was around 1.1 wt. %. The average Pt particle size was determined from TEM micrographs, as well as from H_2 chemisorption. The very small Pt particles in Pt/ZrO_2 could not be detected in TEM because of the limited contrast between Pt and $ZrO_2{\cdot}ZrO_2$ and AlO(OH) without Pt were also studied, these supports had surface areas similar to their respective Pt catalysts.

FTIR spectra of pyridine adsorbed on Pt/ZrO_2 and Pt/AlO(OH) after evacuation at RT and 225 °C and subsequent cooling down to 25 °C are shown in Fig. 1. Peaks of higher intensity can be seen for Pt/ZrO_2 compared to Pt/AlO(OH). Intensities of all of the peaks decreased after evacuation at 225 °C, in particular for Pt/AlO(OH). Based on peak assignments in literature, [27,28] it was concluded that Pt/ZrO_2 has Lewis acidity (LPy; 1605 and 1456 cm^{-1}) and weak Brönsted acidity (BPy; 1641 cm^{-1}), as well as Lewis basicity (LB, Py-ox_1 and Py-ox_2; 1488, 1548 cm^{-1}). This is in agreement with observations of Zaki et al. [28], except for absence of pyridine ν_{19b} mode in the 1540–1500 cm^{-1} region in our study, possibly caused by differences in outgassing procedures. Py-ox_1 and Py-ox_2 were assigned to pyridine oxidation species (carboxylate and carbonaceous species, respectively) based on the observation of Zaki et al. [27] that these species can be formed on metal oxides due to presence of Lewis basic sites at temperatures above 100 °C. For Pt/ZrO_2, pyridine was also found in hydrogen-bonded state (HPy) according to peaks at 1593 and 1442 cm^{-1}.

After evacuation at 225 °C LPy shifted to 1608 cm^{-1}, but BPy almost disappeared suggesting the presence of weak and strong Lewis acid sites and weak Brönsted acid sites. Intensities and rates of disappearance of BPy compared to LPy suggest that Pt/ZrO_2 has more Lewis acid sites than Brönsted acid sites.

Pt/AlO(OH) has Lewis acid sites (LPy; 1616, 1492 cm^{-1}) [27] and no Brönsted acidity, as well as no Lewis basicity which is in agreement with the results of Takagaki et al. [29] However, hydrogen-bonded pyridine was detected as well (HPy; 1595, 1577 and 1446 cm^{-1}). The peak shift of LPy to 1622 cm^{-1} after evacuation at 225 °C suggested that both weak and strong Lewis acid sites are present on Pt/AlO(OH). Pt/AlO(OH) had less intense peaks in all spectra as well as lower surface area compared to Pt/ZrO_2, which suggested a lower surface concentration of Lewis sites on Pt/AlO(OH). Interestingly, acidity of Pt/AlO(OH) is similar to Pt/Al_2O_3 (Fig. S1) despite the differences in Al coordination.

TPD NH_3 profile of Pt/ZrO_2 revealed two peaks at 93 °C and 329 °C (Fig. S2), corresponding to the total acidity of 604 mmol/g. TPD NH_3 profile of Pt/AlO(OH) showed a small peak at 97 °C and a very intense peak at about 500 °C with a shoulder at 300 °C. The total acidity of Pt/AlO(OH) during NH_3 desorption could not be accurately calculated due to interference from H_2O in TCD signal at 500 °C, which is most likely due to water desorbing as a result of phase transformation of AlO(OH) into γ-Al_2O_3 happening at this temperature [30–32].

3.2. In situ ATR-IR results

Fig. 2a shows water subtracted in situ ATR-IR spectra of 2.5 wt.% hydroxyacetone solution flown over a bare ZnSe element at 25 °C, 1 bar. During filling of the cell with the hydroxyacetone solution, the intensity of IR peaks increased gradually and reached saturation within a few minutes. Observed peaks were assigned to different vibrational modes of hydroxyacetone based on literature [33,34]: C═O stretching (1722 cm^{-1}), CO and C—OH coupling (1085 cm^{-1}), C—C stretching (1191 cm^{-1}), H—C—H bending in CH_3 (1427 cm^{-1}), symmetric CH_3 bending (1363 cm^{-1}, C—OH bending (1236 cm^{-1}). The peak at 1635 cm^{-1} is an artifact due to water subtraction and positive peaks between 1600 and 1500 cm^{-1} are caused by increased noise level during the experiment due to moisture leakage around the cell. No other peaks other than those for hydroxyacetone were observed.

Spectra of hydroxyacetone solution at 230 °C, 30 bar (Fig. 2b) were slightly different from spectra at 25 °C. Peaks were less intense and peak positions were slightly shifted. Similarly, no other peaks except for the peaks assigned to hydroxyacetone were observed.

Fig. 3 shows water subtracted in situ ATR-IR spectra collected after 60 min of hydroxyacetone adsorption on Pt/ZrO_2, ZrO_2, Pt/AlO(OH) and AlO(OH) at 25 °C. Spectrum in the absence of the catalyst at 25 °C is also shown, which is identical to the final spectrum in Fig. 2a. Spectra of hydroxyacetone adsorption on Pt/AlO(OH) and AlO(OH) were similar to the ones on bare ZnSe, except for minor peak at 1583 cm^{-1} and less pronounced peak at 1087 cm^{-1}. Peak at 1060 cm^{-1} is assigned to structural hydroxyl groups of boehmite [7,35–37], which were not completely accounted for during background subtraction. This made it difficult to distinguish the peaks of adsorbate species on boehmite surface next to hydroxyacetone in 1150–1000 cm^{-1} spectral region.

Unlike for AlO(OH) samples, two new peaks at 1583 and 1120 cm^{-1} appeared during adsorption on both Pt/ZrO_2 and ZrO_2. The peak positions observed on ZrO_2 and Pt/ZrO_2 were identical, but the intensity

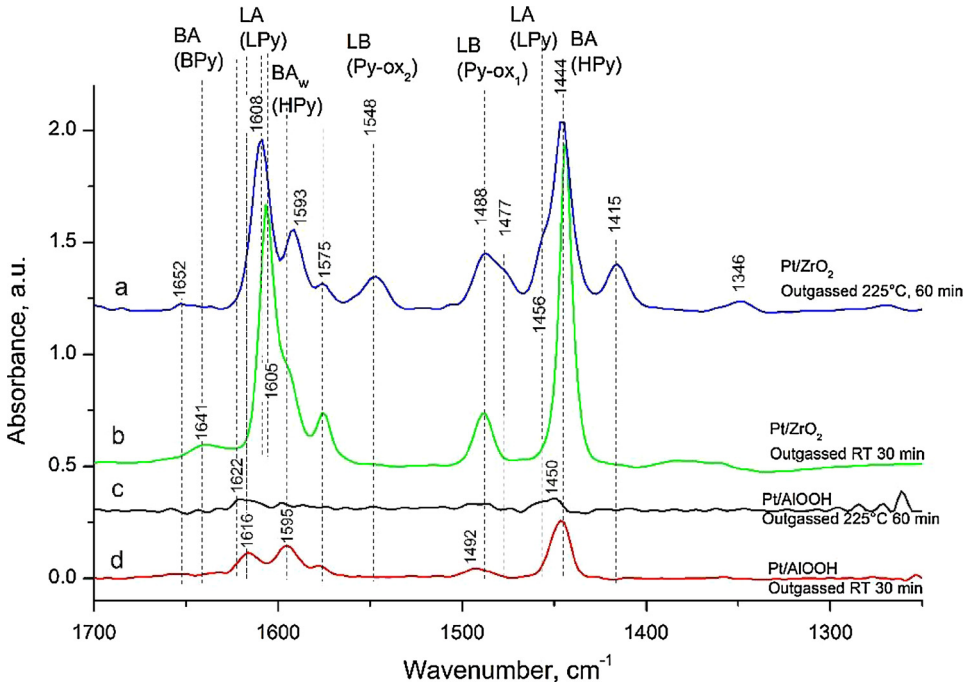

Fig. 1. FTIR spectra after pyridine adsorption on Pt/ZrO_2 (a, b) and Pt/AlO(OH) (c, d) after evacuation at RT (b, d) and 225 °C (a, c).

was significantly higher for ZrO_2. This indicated that same type of adsorbates was formed on the surface of zirconia for both samples. The intensity ratio of 1583 cm^{-1} and 1722 cm^{-1} was much higher for ZrO_2-based samples, than for AlO(OH)-based samples, indicating that higher amounts of adsorbates were formed on ZrO_2-based samples.

Adsorption at 230 °C on ZrO_2-based samples resulted in a few changes in spectra (Fig. 4a), including appearance of shoulders at 1697 and 1679 cm^{-1} next to the peak at 1718 cm^{-1} and broadening of the peak at 1419 cm^{-1}. The peak at 1583 cm^{-1} observed at RT also shifted to lower wavenumber of 1544 cm^{-1}. This may indicate that similar type of adsorbates is formed both at RT and at 230 °C. Interestingly, during initial minutes of the adsorption at 230 °C this region had only a peak at 1604 cm^{-1} which later became dominated by peak at 1544 cm^{-1}. Finally, the quality of the spectra deteriorated by an increasing level of noise, which was caused by leakage of moisture around the cell inside the IR chamber.

Surprisingly, the spectra obtained on AlO(OH) are only mildly influenced by increasing temperature to 230 °C (Fig. 4a). Only the shoulder at 1697 cm^{-1} was observed, whereas no peaks were observed between 1540 and 1600 cm^{-1}. Peaks at 1425 and 1365 cm^{-1} were still well-resolved, suggesting that broadening observed for ZrO_2-based samples was due to surface chemistry on zirconia, and not due to any influence of temperature on the resolution of IR spectra. Adsorbate peaks on Pt/AlO(OH) in the 1150 1000 cm^{-1} region cannot be interpret in detail because the 1060 cm^{-1} peak of boehmite is temperature sensitive.

The spectral region between 2200 and 1800 cm^{-1}, which is typical for CO adsorption on Pt, is shown in Fig. 4b. It is clear that no adsorbed

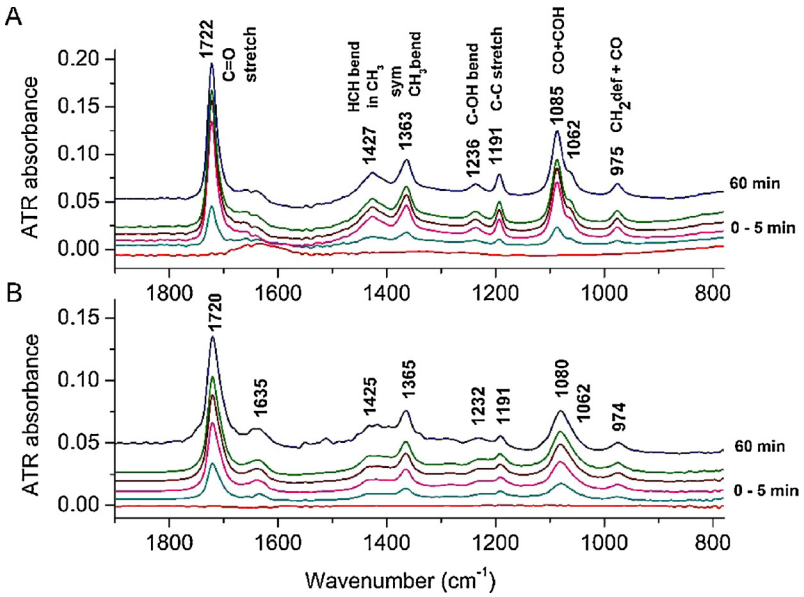

Fig. 2. Water subtracted in situ ATR-IR spectra of hydroxyacetone over bare ZnSe without a catalyst at (a) 25 °C, 1 bar and (b) at 230 °C, 30 bar during 60 min. Spectra with time difference of 1 min are presented during the first 5 min.

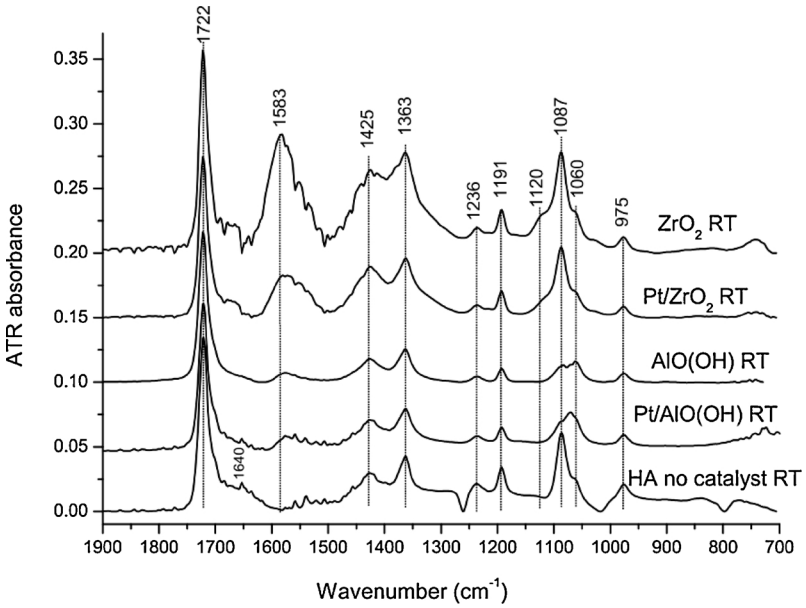

Fig. 3. Water subtracted in situ ATR-IR spectra of hydroxyacetone adsorption on Pt/ZrO_2, ZrO_2, Pt/AlO(OH), AlO(OH) at RT, 1 bar after 60 min.

CO was observed during hydroxyacetone adsorption on both catalysts. However, in a separate experiment where H_2O saturated with CO at 1 bar (26 ppm of CO, feed rate of 10^{-6} mol/min) was flown over the Pt/ZrO_2 catalyst at the same conditions (230 °C, 33 bar), linear and bridge-bonded CO on Pt were observed at 2058 and 1942 cm^{-1}, respectively (Fig. 4b), in agreement with literature [21]. CO adsorption at room temperature resulted in a linearly bound CO on Pt at 2067 cm^{-1} with lower peak intensity compared to 230 °C. No bridge bound CO was observed during adsorption at 25 °C. The intensity of CO peak (2058 cm^{-1}) observed in CO adsorption experiment is approximately 8 times lower than the intensity of the C═O peak of hydroxyacetone (Fig. 4a, no catalyst, 230 °C).

3.2.1. Reactivity of adsorbates during flushing with water: ZrO_2 and Pt/ZrO_2

In order to study the adsorbates on the surface, the catalyst was flushed with water at 230 °C to remove hydroxyacetone in liquid phase (Fig. 5a). Spectra collected during this stage show gradual decrease of hydroxyacetone peaks, however, there were still peaks remaining after flowing water for one hour.

There were two different types of peaks according to their disappearance rate in H_2O: fast disappearing peaks (1718, 1419, 1367, 1191, 1083 and 975 cm^{-1}) belonging to hydroxyacetone in liquid phase and slowly disappearing peaks assigned to adsorbates. Disappearance of hydroxyacetone peaks was similar when flushing the cell with the bare ZnSe crystal at 230 °C (Fig. 5b). The intensities of other peaks (1691, 1593, 1540, 1116 cm^{-1}) in Fig. 5a decreased slower and even stabilized at a certain level. The fact that these peaks did not disappear after 60 min in H_2O in reactive conditions indicated that they belonged to strongly adsorbed and relatively unreactive surface species.

Similar results were obtained for ZrO_2 without Pt as well as for Pt/ZrO_2 at 25 °C and 100 °C after flushing with water for 60 min (results not shown), suggesting that the detected species reside on the ZrO_2 surface, rather than on the Pt particles.

3.3. Coke characterization via elemental analysis and TPO

CHN analysis and temperature programmed oxidation (TPO) was performed to quantify the coke content on catalysts and supports after hydroxyacetone adsorption in the ATR-IR cell, flushing with water and drying, as reported in experimental section. The CHN analysis results presented in Table 1 showed that both Pt/ZrO_2 and Pt/AlO(OH) have 1,6 and 2 times less coke compared to their respective supports, indicating the role of Pt in removing or preventing coke formation. The amount of carbon deposited per m^2 was also significantly different, i.e. 0.11 and 0.07 mg C/m^2 for Pt/ZrO_2 and Pt/AlO(OH), respectively. The tendency of ZrO_2 to form more carbon deposits was therefore not just an effect of surface area.

TPO profile (Fig. 6) of carbonaceous deposits on Pt/ZrO_2 showed one broad peak at 303 °C and small peak around 450 °C, whereas Pt/AlO(OH) showed three overlapping peaks at 286, 338 and 450 °C. The higher intensity of the TPO peaks on Pt/ZrO_2 as compared to Pt/AlO(OH) suggested that more coke was formed on the surface of Pt/ZrO_2, in agreement with the observations based on the elemental analysis (Table 1).

4. Discussion

4.1. Hydroxyacetone adsorption

Adsorption of hydroxyacetone at room temperature (Fig. 3) on zirconia results in the appearance of two new peaks compared to dissolved hydroxyacetone, i.e. at 1583 and 1087 cm^{-1}. The fact that the peak positions do not depend on the presence of Pt indicates that these new peaks are to be assigned to adsorbed species on the zirconia surface. At this point it is not clear whether chemisorbed hydroxyacetone or condensation products of hydroxyacetone, as discussed below in more detail for experiments at 230 °C, are responsible.

The spectra collected during exposure of Pt/ZrO_2 to hydroxyacetone solution at 230 °C were curve fitted with peaks positioned at 1718, 1541, 1604, 1123 and 1083 cm^{-1}, and evolution of peak areas is shown in Fig. 7. Note that the spectrum resulting in the datapoints at 60 min is presented in Fig. 4a. The intensity of peaks of hydroxyacetone in liquid phase (1718 and 1083 cm^{-1}) increased after an initial delay of 5 min, stabilizing after 30 min.

Peaks assigned to adsorbates at 1120, 1604 and 1541 cm^{-1} appeared after 5 min and continued to increase until 10 min. The initial delay of 5 min is caused by the residence time in the feed lines and the preheater, upstream of the cell. The peak at 1604 cm^{-1} dominated over 1541 cm^{-1} during the first 10 minutes, however after 10 minutes the intensity of 1541 cm^{-1} increased further, and the intensity of 1604 cm^{-1} decreased significantly. The profile of 1604 cm^{-1} is typical

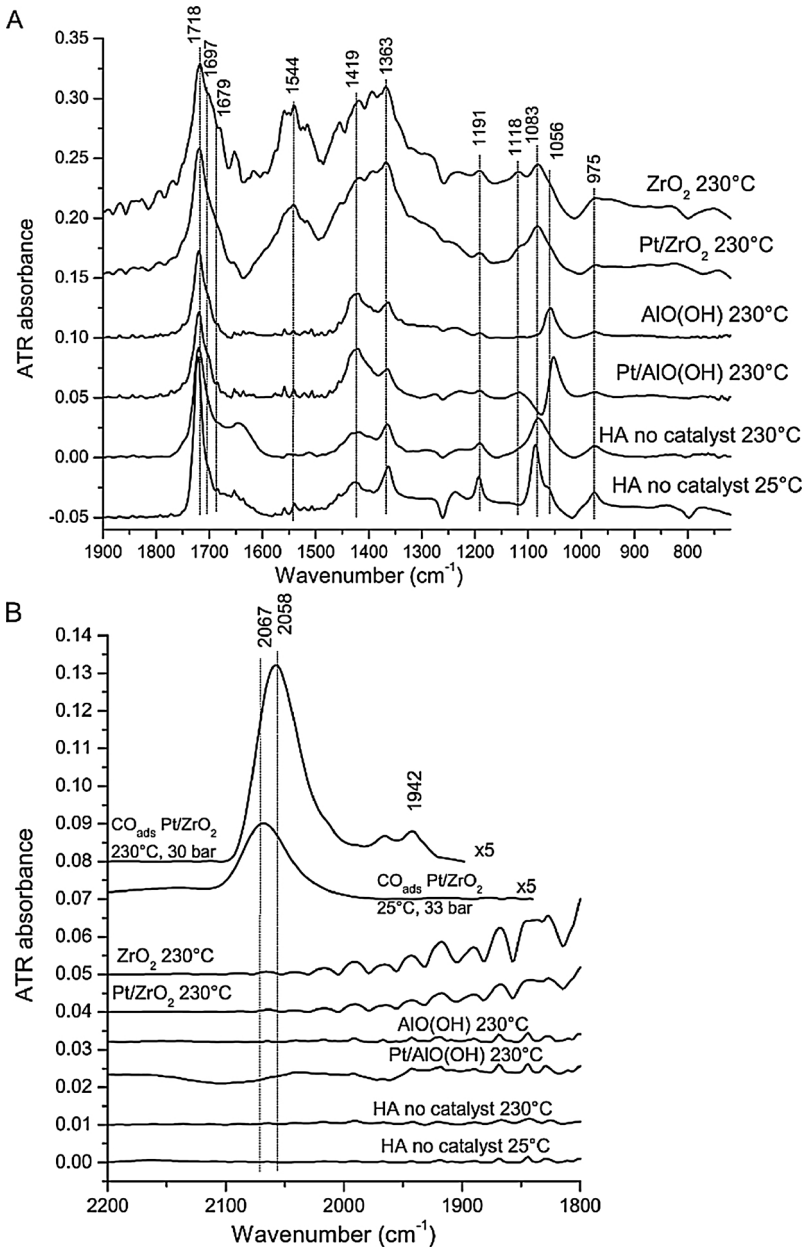

Fig. 4. Water subtracted in situ ATR-IR spectra of hydroxyacetone adsorption on Pt/ZrO_2, ZrO_2, $Pt/AlO(OH)$, $AlO(OH)$ at 230 °C, 30 bar after 60 min in the frequency range (a) 1900–720 cm^{-1}, (b) 2200–1800 cm^{-1}. ATR-IR adsorption spectra of CO adsorbed on Pt/ZrO_2 from CO dissolved in water at 25 °C, 33 bar and 230 °C, 30 bar after 60 min are added for comparison. Intensities of the peaks of adsorbed CO were multiplied by 5 times for clarity.

for intermediate product profile in a sequential reaction. An assignment of this peak to a potential intermediate will be discussed in Section 4.3.

4.2. Flushing with water

Spectra presented in Fig. 5a were fitted with a set of peaks similar to the ones used to construct Fig. 7 during adsorption step (1718, 1691, 1541, 1120, 1057 cm^{-1}). Results of the fitting are presented in Fig. 8 for the case of Pt/ZrO_2. Similar results were obtained in the case of ZrO_2 (not shown).

The peaks assigned to hydroxyacetone in the liquid phase (1718 and 1083 cm^{-1}, Fig. 8) decrease much faster in intensity than the peaks assigned to adsorbates. The fact that adsorbate peak areas decreased slightly or did not decrease at all indicated that these were strongly adsorbed on the surface. The slight decrease in peak area may be explained by consecutive reactions of adsorbates with water that can take place at these conditions, although slow desorption cannot be ruled out.

4.3. Identification of adsorbed species

In order to determine the origin of the new peaks at 1691, 1593, 1540, 1116 and 1055 cm^{-1} possible reactions of hydroxyacetone were considered. Peak positions indicate that adsorbates may contain carbonyl and unsaturated carbon-carbon bonds. Apart from reforming reaction, hydroxyacetone can undergo enolization and aldol condensation reactions.

IR frequencies of the two enols of hydroxyacetone (prop-1-ene-1,2-diol and prop-2-ene-1,2-diol) were calculated using DFT-based method, which was validated on the grounds of the good agreement between calculated and experimental spectrum of hydroxyacetone (Table S1). The influence of water molecules on hydroxyacetone spectrum was found to be negligible based on minor frequency shifts and intensity

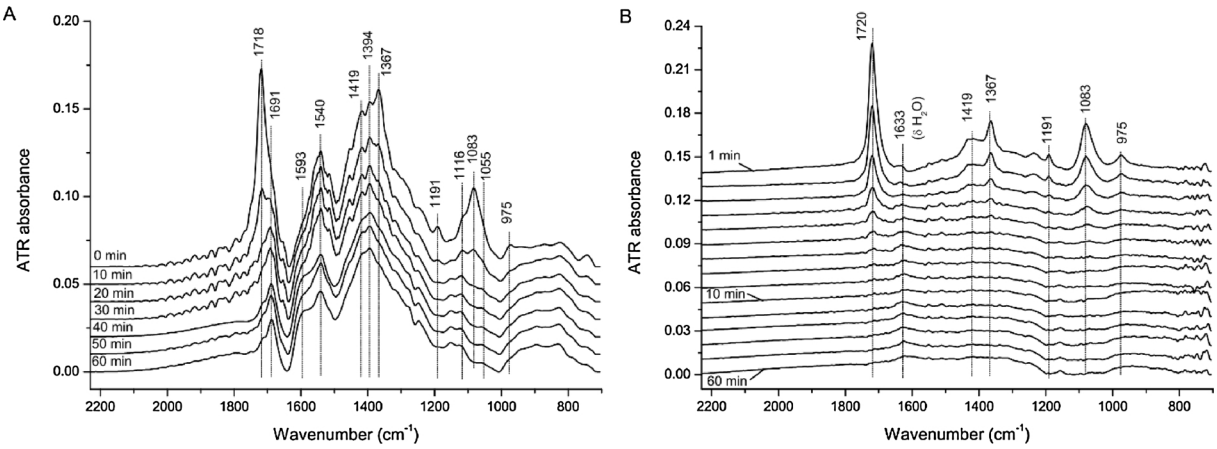

Fig. 5. Time resolved water corrected in situ ATR-IR spectra during hydroxyacetone removal with H_2O at 230 °C, 30 bar on (a) Pt/ZrO_2, (b) bare ZnSe element. Spectra with time difference of 10 min are presented during 60 min. Spectrum at 0 min in (a) is identical to Pt/ZrO_2 spectrum on Fig. 2.

Table 1
Elemental analysis of samples after ATR-IR experiments, including hydroxyacetone adsorption, flushing with water and drying.

Catalyst	Elemental composition, wt.%	
	C	H
Pt/AlO(OH)	0.27	
Pt/ZrO_2	1.05	0.32
AlO(OH)	0.50	
ZrO_2	1.61	0.38

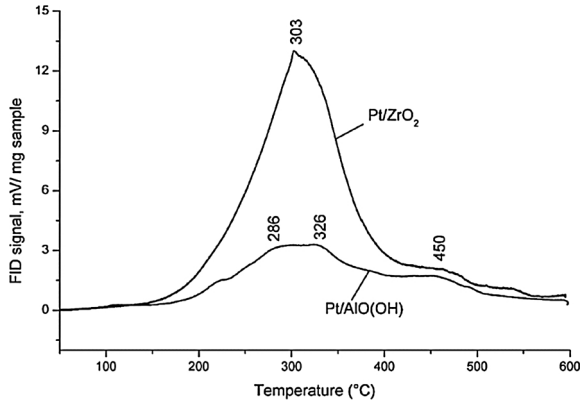

Fig. 6. TPO profiles of Pt/ZrO_2 and Pt/AlO(OH) after ATR-IR experiment, which included hydroxyacetone adsorption, flushing with water and drying.

changes.

Calculated frequencies for enols in vacuum do not match with the experimentally observed frequencies on Pt/ZrO_2 at 230 °C, suggesting that adsorbed species do not include enols. This qualitatively agrees with a DFT study on adsorption, tautomerization and decomposition of acetone on Pt (111) surface by Xu et al. [38] reporting that only a small amount of acetone could tautomerize into enol Pt (111) surface at room temperature. Low extent of enolization of hydroxyacetone in D_2O and in triethylamine solution was also reported by Yaylayan et al. [34]

Two products of aldol condensation can be formed from the two considered enols (Fig. 9) - (Z)-3,5-dihydroxy-4-methylpent-3-en-2-one (3,5-DH) and (Z)-1,5-dihydroxy-4-methylpent-3-en-2-one (1,5-DH), via 3,4,5-trihydroxy-4-methylpentan-2-one and 1,4,5-trihydroxy-4-methylpentan-2-one as intermediate products. It may be speculated that the rapid increase in intensity of the peak at 1604 cm^{-1} is due to one of these intermediate products. Interestingly, similar assignments were proposed by Zaki et al. [28] for aldol condensation of acetone on zirconia and alumina surfaces.

Infrared spectra of the most stable conformations for both aldol condensation products in vacuum and in the presence of water were also calculated (Table S1). The influence of water can be summarized with a frequency decrease of about 30 cm^{-1} for the peaks located in the region comprised between 1500 and 1700 cm^{-1}. At a molecular level this is due to the elongation of the C═O bond caused by hydrogen bonds and to the delocalization of the C═O and C═C coupled stretching vibrations on the microsolvation water molecules. Comparison of the most important vibrational frequencies of both dimers in vacuum and in the presence of water with experimental data is given in Table 2.

The calculated spectra of the two condensation products are similar in the region of C═O and C═C vibrations, both having two coupled stretching vibrations around 1680 and 1600–1630 cm^{-1}. The coupling with the C═C stretching determines the shift of the C═O band to lower frequencies. Analysis of the deviations in peak positions and intensities (deviations are given in the brackets in Table 2) for both dimers shows good agreement with experimental results. These deviations are within the estimated accuracy of the calculation method. The calculated C═O frequency in the presence of water is shifted by around 2% compared to experimentally observed frequency. The comparison of C═C frequency is less clear, since two peaks at 1593 and 1540 cm^{-1} were observed in the experimental spectrum and deviations between theory and experiment are somewhat larger.

Dimers 3,5-DH and 1,5-DH can be distinguished based on the vibrational band at 1086 cm^{-1} or 1071 cm^{-1} when corrected for water. This peak is absent in the spectrum of 3,5-DH as well as in the experimental spectrum (Fig. 5a); thus, 3,5-DH seems to be the dominant aldol condensation product of hydroxyacetone. The absence of this band is attributed to the presence of a hydrogen bond between the hydroxyl groups in 3,5DH that determines the shift of the C–OH stretching band to the lower frequencies (1044–1025 cm^{-1}).

4.4. Nature of the support in aldol condensation

The different IR adsorption spectra for Pt/ZrO_2 and Pt/AlO(OH) presented in Fig. 4a suggested that aldol condensation, as discussed in the previous section, does not occur on the surface of boehmite. This is probably due to the lower surface acidity of boehmite compared to zirconia. TPD NH_3 results (Fig. S2) showed that total acidity of zirconia is higher than boehmite. Pyridine adsorption measured with IR (Fig. 1) also suggested that Pt/ZrO_2 has high concentration of Lewis and Brönsted acid sites and Lewis basic sites, while Pt/AlO(OH) has low concentration of Lewis acid sites. It was suggested in literature [28,39,40] that zirconia can catalyze aldol condensation of acetone,

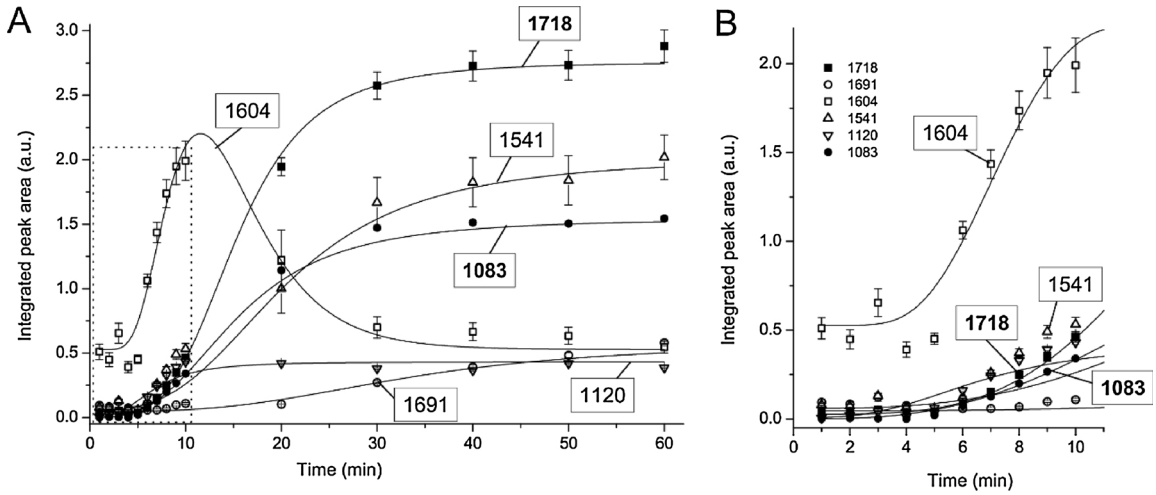

Fig. 7. Integrated areas of peaks assigned to hydroxyacetone (1718 cm^{-1} and 1083 cm^{-1}) and peaks assigned to adsorbates at 1691 cm^{-1}, 1541 cm^{-1}, 1604 cm^{-1} and 1120 cm^{-1} during initial adsorption of hydroxyacetone on Pt/ZrO_2 at 230 °C, 30 bar, showing time (a) 0–60 min, (b) zoomed to first 10 min. Error bars represent fitting error, the lines are presented to guide the eye.

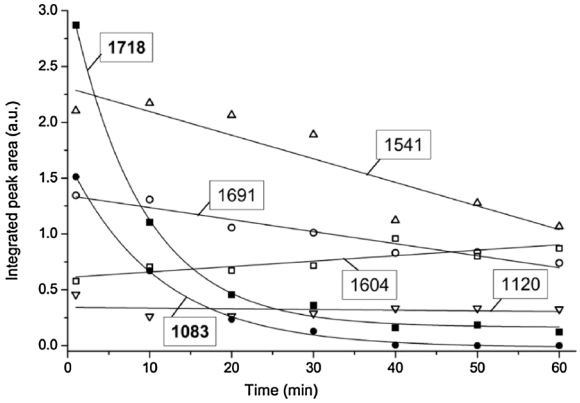

Fig. 8. Integrated areas of peaks at 1718 cm^{-1} and 1083 cm^{-1} assigned to hydroxyacetone and peaks at 1691, 1604, 1541 and 1120 cm^{-1} assigned to adsorbates while hydroxyacetone is being washed out from the cell with Pt/ZrO_2 at 230 °C, 30 bar during 60 min. The lines are presented to guide the eye.

due to its Lewis basicity. Thus, the condensation would proceed according to the mechanism suggested in Fig. 9. However, since acidity of boehmite and γ-Al_2O_3 is similar, based on the pyridine desorption data, one can assume that boehmite may also catalyze aldol condensation via an acidic route. In fact, Ferri et al. [41] reported aldol condensation of ethyl pyruvate catalyzed by alumina, and Dumitriu et al. [42] studied aldol condensation of acetaldehyde on MFI zeolites. Our IR results, however, do not indicate formation of any condensation products on boehmite under APR conditions.

Possibly, condensation products are not detected on AlO(OH) supported catalyst because Pt/AlO(OH) is more active in formation of gaseous reforming products (CO_x, H_2, etc.) than Pt/ZrO_2; as reforming to CO_x competes with condensation reactions, this may well contribute to the difference in the formation of condensation products between AlO(OH) and ZrO_2. Ongoing work in the group indeed confirms that Pt/AlO(OH) is more stable and forms less carbonaceous deposits than Pt/ZrO_2 (to be published).

4.5. Adsorbed CO – water gas shift reaction

In Fig. 4b no CO peak was seen in the region where linearly adsorbed CO on Pt is usually expected. Clearly, the absence of CO in the spectra during exposure to hydroxyacetone at 230 °C was not due to limited sensitivity of the technique, since chemisorbed CO was easily observable when H_2O saturated with CO was flown over Pt/ZrO_2 at 25 °C and 230 °C (top two spectra, Fig. 2b).

He et al. [43] have reported on formation of adsorbed CO on 2,1 wt. % Pt/Al_2O_3 catalyst during APR of methanol in liquid phase at 150 °C, 584 bar. CO coverage of 0.29 and 0.4 on Pt was observed for liquid phase reforming of 2 and 5 wt. % methanol, respectively. Similar results were obtained by Wawrzetz et al. [44] in APR of 20 wt.% glycerol on 3 wt.% Pt/Al_2O_3 at 225 °C, 29 bar. Two small peaks at 2050 and

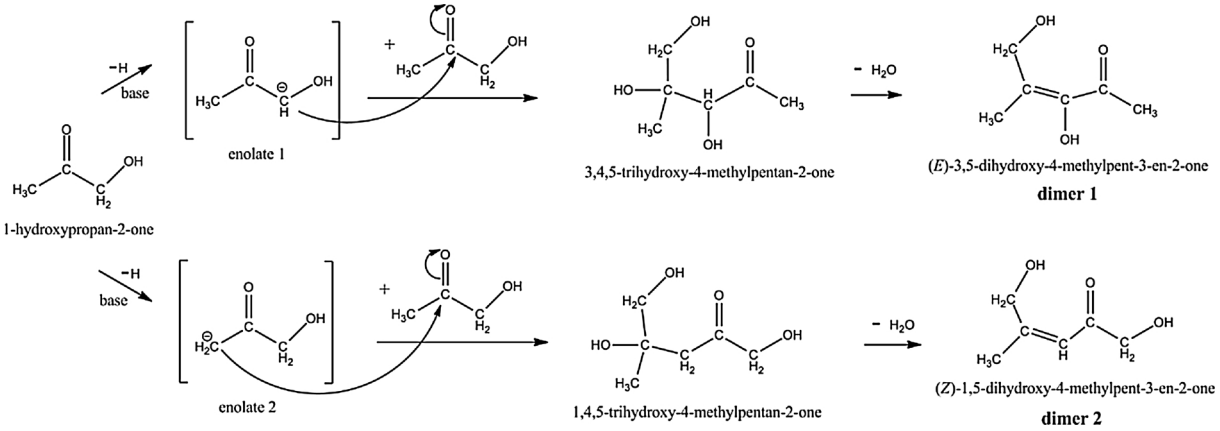

Fig. 9. Two possible pathways of aldol condensation of hydroxyacetone.

Table 2
Comparison of experimental frequencies (last spectrum in Fig. 5a) with calculated frequencies of aldol condensation products of hydroxyacetone in vacuum and in the presence of six water molecules.

Experimental frequencies, cm^{-1}	1691 (s)[a]	1593 (ms)	1540 (s)	1380 (vs)	1116 (w)	–	1055 (w)
Calculated frequencies, cm^{-1}:							
3,5-DH in vacuum	1684 (s) (−0.4 %)[b]	1637 (vs) (2.8 %)	1637 (vs) (6.3 %)	1370 (s) (−0.7 %)	1123 (s) (0.6 %)	–	1044 (ms) (−1.0 %)
3,5-DH surrounded by $6H_2O$ molecules	1654 (w) (−2.2 %)	1611 (vs) (1.1 %)	1611 (vs) (4.4 %)	1355 (s) (−1.8 %)	1115 (s) (−0.1 %)	–	1037 (s) (−1.7 %)
1,5-DH in vacuum	1687 (s) (−0.2 %)	1608 (vs) (0.9 %)	1608 (vs) (4.4 %)	1401 (s) (1.5 %)	1129 (ms) (1.2 %)	1086 (vs)	1056 (ms) (0.1 %)
1,5-DH surrounded by $6H_2O$ molecules	1651 (s) (−2.4 %)	1587 (vs) (−0.4 %)	1587 (vs) (3.1 %)	1396 (s) (1.2 %)	1128 (ms) (1.1 %)	1071 (vs)	1058 (w) 0.3 %)

[a] Intensities of the peaks are presented as (vs) very strong, (s) strong, (ms) medium strong, (w) weak.
[b] Deviations of calculated frequencies from experimental frequencies are given in the brackets. Peak assignments: 1691 cm^{-1} - asymmetric stretching of C═O and C═C coupled vibrations, 1593 and 1540 cm^{-1} - symmetric stretching of C═O and C═C coupled vibrations, 1116 cm^{-1} −C−H bending in C═CH, 1055 cm^{-1} - coupled C−OH stretching.

1940 cm^{-1} were observed in the ATR-IR spectra [44], which were assigned to linear and bridge bound CO on Pt. However, this assignment can be debated because boehmite, which was formed from alumina during APR, has IR peaks in the same window. Copeland et al. [25] have studied activation of glycerol on 5 wt. % Pt/Al_2O_3 using ATR-IR spectroscopy at room temperature. Formation of two types of adsorbed CO was reported (i) CO interacting with co-adsorbed H_2 and (ii) CO interacting with molecularly adsorbed H_2O. The authors emphasized that the rates of CO formation and consumption strongly depend on the cleaning procedure of the catalyst layer prior to kinetic studies. The cleaning pretreatment in this study included alternating flows of H_2- and O_2-saturated water, identical in the study by Copeland et al. [25]

The absence of adsorbed CO in the APR experiment in the ATR-IR cell is suggesting that on Pt/AlO(OH) adsorbed CO is not involved in the rate-determining step in APR of hydroxyacetone; in other words, formation of adsorbed CO is relatively slow as compared to desorption, water gas shift and methanation, i.e. all reactions that would consume adsorbed CO. The same cannot be concluded for Pt/ZrO_2 considering the fast and complete deactivation for gasification (results of the ongoing work to be published). Therefore, it is quite possible that the absence of adsorbed CO is explained by deactivation of the catalyst in this case. Clearly, these conclusions are valid for experiments at conversion levels well below 1%. Unfortunately, it was not possible to confirm gasification activity during the ATR-IR experiment experimentally.

4.6. Deactivation of the catalysts due to coke formation

TPO analysis of the samples after hydroxyacetone adsorption in the ATR-IR cell (Fig. 6) showed higher peak intensities for Pt/ZrO_2 compared to Pt/AlO(OH), suggesting higher amount of coke on Pt/ZrO_2. Two different regions of oxidation temperatures around 300 °C and 450 °C were observed for both samples, with Pt/ZrO_2 having most of the coke burning at lower temperatures. Elemental analysis of the same samples (Table 1) showed the highest amount of coke on ZrO_2 sample, and the lowest coke amount on Pt/AlO(OH), which is in agreement with TPO results. The amount of coke on supports was higher than on Pt/support samples. These results suggest that reactions on the surface of supports are possibly causing the accumulation of coke. The aldol condensation reaction is probably the first step in this sequence, since it leads to formation of molecules with long unsaturated carbon chains. Oxidation temperatures of carbon deposits for Pt/ZrO_2 are well below the oxidation temperatures of hydrocarbon coke that is observed in e.g. methane dry reforming [45–47], suggesting that coke on Pt/ZrO_2 is a "soft" coke with high oxygen content.

Thus, aldol condensation of hydroxyacetone, resulting in formation of (E)-3,5-dihydroxy-4-methylpent-3-en-2-one, is likely to be the first step in the formation of oxygen rich deposits, significantly responsible for the catalyst deactivation in aqueous phase reforming of hydroxyacetone. The reforming reaction that takes place on Pt surface is competing with the condensation reaction; however, the acid-base properties of the support clearly influences the condensation reactions, leading to coke formation independent of the presence of Pt.

5. Conclusions

In situ Attenuated Total Reflection Infrared (ATR-IR) spectroscopy allows to study adsorbed species that form during exposure to hydroxyacetone on Pt/AlO(OH) and Pt/ZrO_2 catalysts under conditions of aqueous phase reforming, i.e. 230 °C/30 bar. In addition to reforming reaction, hydroxyacetone undergoes aldol condensation resulting in strongly adsorbed species when brought in contact with ZrO_2-based catalyst due to the presence of Lewis acid and basic sites; the dominant pathway of aldol condensation was identified. However, no condensation products were observed on AlO(OH)-based catalyst due to its weak Lewis acidity. Oxygen-rich carbonaceous deposits are formed on zirconia via condensation of hydroxyacetone, leading to catalyst deactivation. Additionally, absence of adsorbed CO in the spectra suggests that conversion and desorption of CO chemisorbed on Pt is not rate-limiting.

Acknowledgements

This research has been performed within the framework of the CatchBio program (project number 053.70.002). The authors gratefully acknowledge the support of the Smart Mix Program of the Netherlands Ministry of Economic Affairs and the Netherlands Ministry of Education, Culture and Science. The authors thank Tom Velthuizen and Karin Altena - Schildkamp for BET and XRF analyses, Ing. Bert Geerdink for technical help in building the ATR-IR setup. K. Koichumanova thanks Erik Dietrich for help with data processing in Matlab.

Appendix A. Supplementary data

Supplementary material related to this article can be found, in the online version, at doi:https://doi.org/10.1016/j.apcatb.2018.03.090.

References

[1] R.D. Cortright, R.R. Davda, J.A. Dumesic, Hydrogen from catalytic reforming of biomass-derived hydrocarbons in liquid water, Nature 418 (6901) (2002) 964–967.
[2] G.W. Huber, J.W. Shabaker, J.A. Dumesic, Raney Ni-Sn catalyst for H-2 production from biomass-derived hydrocarbons, Science 300 (5628) (2003) 2075–2077.
[3] R.R. Davda, R. Alcalá, J. Shabaker, G. Huber, R.D. Cortright, M. Mavrikakis, J.A. Dumesic, 11 DFT and experimental studies of C−C and C−O bond cleavage in ethanol and ethylene glycol on Pt catalysts, Stud. Surf. Sci. Catal. 145 (2003) 79–84.
[4] R.R. Davda, J.W. Shabaker, G.W. Huber, R.D. Cortright, J.A. Dumesic, A review of

catalytic issues and process conditions for renewable hydrogen and alkanes by aqueous-phase reforming of oxygenated hydrocarbons over supported metal catalysts, Appl. Catal. B-Environ. 56 (1–2) (2005) 171–186.
[5] D.J.M. De Vlieger, B.L. Mojet, L. Lefferts, K. Seshan, Aqueous phase reforming of ethylene glycol - role of intermediates in catalyst performance, J. Catal. 292 (2012) 239–245.
[6] K. Koichumanova, A.K.K. Vikla, D.J.M. de Vlieger, K. Seshan, B.L. Mojet, L. Lefferts, Towards stable catalysts for aqueous phase conversion of ethylene glycol for renewable hydrogen, Chemsuschem 6 (9) (2013) 1717–1723.
[7] K. Koichumanova, K.B. Sai Sankar Gupta, L. Lefferts, B.L. Mojet, K. Seshan, An in situ ATR-IR spectroscopy study of aluminas under aqueous phase reforming conditions, Phys. Chem. Chem. Phys. 17 (37) (2015) 23795–23804.
[8] D.J.M. DeVlieger, D.B. Thakur, L. Lefferts, K. Seshan, Carbon nanotubes: a promising catalyst support material for supercritical water gasification of biomass waste, ChemCatChem 4 (12) (2012) 2068–2074.
[9] D.J.M. De Vlieger, L. Lefferts, K. Seshan, Ru decorated carbon nanotubes-a promising catalyst for reforming bio-based acetic acid in the aqueous phase, Green. Chem. 16 (2) (2014) 864–874.
[10] A. Ciftci, D.A.J. Michel, E.J.M. Hensen, Influence of Pt particle size and Re addition by catalytic Reduction on aqueous phase reforming of glycerol for carbon-supported Pt(Re) catalysts, Appl. Catal. B: Environ. 174–175 (2015) 126–135.
[11] I. Coronado, M. Stekrova, M. Reinikainen, P. Simell, L. Lefferts, J. Lehtonen, A review of catalytic aqueous-phase reforming of oxygenated hydrocarbons derived from biorefinery water fractions, Int. J. Hydrog. Energy 41 (26) (2016) 11003–11032.
[12] A. Oasmaa, D. Meier, Norms and standards for fast pyrolysis liquids: 1. Round robin test, J. Anal. Appl. Pyrolysis 73 (2) (2005) 323–334.
[13] C.R. Vitasari, G.W. Meindersma, A.B. de Haan, Water extraction of pyrolysis oil: the first step for the recovery of renewable chemicals, Bioresour. Technol. 102 (14) (2011) 7204–7210.
[14] R. Trane-Restrup, D.E. Resasco, A.D. Jensen, Steam reforming of light oxygenates, Catal. Sci. Technol. 3 (12) (2013) 3292–3302.
[15] F. Bimbela, M. Oliva, J. Ruiz, L. García, J. Arauzo, Catalytic steam reforming of model compounds of biomass pyrolysis liquids in fixed bed: acetol and n-butanol, J. Anal. Appl. Pyrolysis 85 (1-2) (2009) 204–213.
[16] M.C. Ramos, A.I. Navascués, L. García, R. Bilbao, Hydrogen production by catalytic steam reforming of acetol, a model compound of bio-oil, Ind. Eng. Chem. Res. 46 (8) (2007) 2399–2406.
[17] J.A. Medrano, M. Oliva, J. Ruiz, L. García, J. Arauzo, Catalytic steam reforming of model compounds of biomass pyrolysis liquids in fluidized bed reactor with modified Ni/Al catalysts, J. Anal. Appl. Pyrolysis 85 (1–2) (2009) 214–225.
[18] V.R. Dubey, P.D. Vaidya, Kinetics of steam reforming of acetol over a Pt/C catalyst, Chem. Eng. J. 180 (2012) 263–269.
[19] S.H. Hakim, B.H. Shanks, J.A. Dumesic, Catalytic upgrading of the light fraction of a simulated bio-oil over CeZrOx catalyst, Appl. Catal. B: Environ. 142–143 (2013) 368–376.
[20] J. Ryczkowski, IR spectroscopy in catalysis, Catal. Today 68 (4) (2001).
[21] B.L. Mojet, S.D. Ebbesen, L. Lefferts, Light at the interface: the potential of attenuated total reflection infrared spectroscopy for understanding heterogeneous catalysis in water, Chem. Soc. Rev. 39 (12) (2010) 4643–4655.
[22] T. Bürgi, A. Baiker, Attenuated total reflection infrared spectroscopy of solid catalysts functioning in the presence of liquid-phase reactants, in: C.G. Bruce, K. Helmut (Eds.), Advances in Catalysis, vol. 50, Academic Press, 2006, pp. 227–283.
[23] J.M. Andanson, A. Baiker, Exploring catalytic solid/liquid interfaces by in situ attenuated total reflection infrared spectroscopy, Chem. Soc. Rev. 39 (12) (2010) 4571–4584.
[24] K. Koichumanova, A. Visan, B. Geerdink, R.G.H. Lammertink, B.L. Mojet, K. Seshan, L. Lefferts, ATR-IR spectroscopic cell for in situ studies at solid-liquid interface at elevated temperatures and pressures, Catal. Today 283 (2017) 185–194.
[25] J.R. Copeland, G.S. Foo, L.A. Harrison, C. Sievers, In situ ATR-IR study on aqueous phase reforming reactions of glycerol over a Pt/γ-Al2O3 catalyst, Catal. Today 205 (0) (2013) 49–59.
[26] M.J. Frisch, Gaussian 09, Gaussian, Inc, Wallingford, CT, USA, 2009.
[27] M.I. Zaki, M.A. Hasan, F.A. Al-Sagheer, L. Pasupulety, In situ FTIR spectra of pyridine adsorbed on SiO2-Al2O3, TiO2, ZrO2 and CeO2: general considerations for the identification of acid sites on surfaces of finely divided metal oxides, Colloids Surf. A Physicochem. Eng. Asp. 190 (3) (2001) 261–274.
[28] M.I. Zaki, M.A. Hasan, L. Pasupulety, Surface reactions of acetone on Al2O3, TiO2, ZrO2, and CeO2: IR spectroscopic assessment of impacts of the surface acid-base properties, Langmuir 17 (3) (2001) 768–774.
[29] A. Takagaki, J.C. Jung, S. Hayashi, Solid Lewis acidity of boehmite γ-AlO(OH) and its catalytic activity for transformation of sugars in water, RSC Adv. 4 (82) (2014) 43785–43791.
[30] G. Krishna Priya, P. Padmaja, K.G.K. Warrier, A.D. Damodaran, G. Aruldhas, Dehydroxylation and high temperature phase formation in sol-gel boehmite characterized by Fourier transform infrared spectroscopy, J. Mater. Sci. Lett. 16 (19) (1997) 1584–1587.
[31] T. Tsukada, H. Segawa, A. Yasumori, K. Okada, Crystallinity of boehmite and its effect on the phase transition temperature of alumina, J. Mater. Chem. 9 (2) (1999) 549–553.
[32] X. Krokidis, P. Raybaud, A.E. Gobichon, B. Rebours, P. Euzen, H. Toulhoat, Theoretical study of the dehydration process of boehmite to γ-alumina, J. Phys. Chem. B 105 (22) (2001) 5121–5130.
[33] V. Mohaček-Grošev, Vibrational analysis of hydroxyacetone, Spectrochim. Acta Part A: Mol. Biomol. Spectrosc. 61 (3) (2005) 477–484.
[34] V.A. Yaylayan, S. Harty-Majors, A.A. Ismail, Monitoring carbonyl-amine reaction and enolization of 1-hydroxy-2- propanone (acetol) by FTIR spectroscopy, J. Agric. Food Chem. 47 (6) (1999) 2335–2340.
[35] S.A. Dickie, A.J. McQuillan, In-situ infrared spectroscopic studies of adsorption processes on boehmite particle films: exchange of surface hydroxyl groups observed upon chelation by acetylacetone, Langmuir 20 (26) (2004) 11630–11636.
[36] D. Tunega, H. Pasalic, M.H. Gerzabek, H. Lischka, Theoretical study of structural, mechanical and spectroscopic properties of boehmite (gamma-AlOOH), J. Phys. Condens Matter 23 (40) (2011) 404201.
[37] S. Ram, Infrared spectral study of molecular vibrations in amorphous, nanocrystalline and AlO(OH) · αH2O bulk crystals, Infrared Phys. Technol. 42 (6) (2001) 547–560.
[38] M. Xu, X.L. Huai, H. Liu, Role of keto-enol isomerization on surface chemistry and hydrogenation of acetone on pt(111): a DFT study, Ind. Eng. Chem. Res. 53 (13) (2014) 5451–5454.
[39] V. Crocellà, G. Cerrato, C. Morterra, On the adsorption/reaction of acetone on pure and sulfate-modified zirconias, Phys. Chem. Chem. Phys. 15 (32) (2013) 13446–13461.
[40] M.I. Zaki, M.A. Hasan, F.A. Al-Sagheer, L. Pasupulety, Surface chemistry of acetone on metal oxides: IR observation of acetone adsorption and consequent surface reactions on silica-alumina versus silica and alumina, Langmuir 16 (2) (2000) 430–436.
[41] D. Ferri, S. Diezi, M. Maciejewski, A. Baiker, Alumina-catalysed degradation of ethyl pyruvate during enantioselective hydrogenation over Pt/alumina and its inhibition by acetic acid, Appl. Catal. A-Gen. 297 (2) (2006) 165–173.
[42] E. Dumitriu, V. Hulea, I. Fechete, A. Auroux, J.-F. Lacaze, C. Guimon, The aldol condensation of lower aldehydes over MFI zeolites with different acidic properties, Microporous Mesoporous Mater. 43 (3) (2001) 341–359.
[43] R. He, R.R. Davda, J.A. Dumesic, In situ ATR-IR spectroscopic and reaction kinetics studies of water-gas shift and methanol reforming on Pt/Al2O3 catalysts in vapor and liquid phases, J. Phys. Chem. B 109 (7) (2005) 2810–2820.
[44] A. Wawrzetz, B. Peng, A. Hrabar, A. Jentys, A.A. Lemonidou, J.A. Lercher, Towards understanding the bifunctional hydrodeoxygenation and aqueous phase reforming of glycerol, J. Catal. 269 (2) (2010) 411–420.
[45] J. Guo, H. Lou, H. Zhao, D. Chai, X. Zheng, Dry reforming of methane over nickel catalysts supported on magnesium aluminate spinels, Appl. Catal. A 273 (1–2) (2004) 75–82.
[46] J. Guo, H. Lou, X. Zheng, The deposition of coke from methane on a Ni/MgAl2O4 catalyst, Carbon 45 (6) (2007) 1314–1321.
[47] A.I. Tsyganok, T. Tsunoda, S. Hamakawa, K. Suzuki, K. Takehira, T. Hayakawa, Dry reforming of methane over catalysts derived from nickel-containing Mg-Al layered double hydroxides, J. Catal. 213 (2) (2003) 191–203.